




Cite this: *Phys. Chem. Chem. Phys.*,  
2022, 24, 14680

# Computational approaches for XANES, VtC-XES, and RIXS using linear-response time-dependent density functional theory based methods

Daniel R. Nascimento\*<sup>a</sup> and Niranjana Govind \*<sup>b</sup>

The emergence of state-of-the-art X-ray light sources has paved the way for novel spectroscopies that take advantage of their atomic specificity to shed light on fundamental physical, chemical, and biological processes both in the static and time domains. The success of these experiments hinges on the ability to interpret and predict core-level spectra, which has opened avenues for theory to play a key role. Over the last two decades, linear-response time-dependent density functional theory (LR-TDDFT), despite various theoretical challenges, has become a computationally attractive and versatile framework to study excited-state spectra including X-ray spectroscopies. In this context, we focus our discussion on LR-TDDFT approaches for the computation of X-ray Near-Edge Structure (XANES), Valence-to-Core X-ray Emission (VtC-XES), and Resonant Inelastic X-ray Scattering (RIXS) spectroscopies in molecular systems with an emphasis on Gaussian basis set implementations. We illustrate these approaches with applications and provide a brief outlook of possible new directions.

Received 8th March 2022,  
Accepted 6th June 2022

DOI: 10.1039/d2cp01132h

[rsc.li/pccp](http://rsc.li/pccp)

## 1 Introduction

X-ray spectroscopies are quickly becoming essential experimental techniques for the chemical characterization of molecules and materials. Their main advantage results from the localized nature of the orbitals from which electrons are excited, which leads to spectral features that are atom-specific and highly sensitive to their chemical environment.<sup>1–4</sup> Thus, the spectral features involving electronic transitions in the X-ray region contain valuable structural information.

Recent advances in light-source technologies<sup>5</sup> have resulted in immense improvements in the temporal and energy resolution that can be obtained from X-ray spectroscopies, broadening its domain of applicability. In addition, the development of laboratory-based X-ray spectroscopies<sup>6</sup> has added to this growing trend. These advances have also resulted in an increased demand for inexpensive computational approaches that can aid in the interpretation of complex spectroscopic features and help the design of new experiments.

Single-photon X-ray spectroscopies (X-ray absorption and emission) can be modeled with a wide range of quantum chemical techniques ranging from simplistic single-reference wavefunction-based approaches to elaborate multi-reference

methods. In recent years, considerable progress has been made in the development of highly-accurate methods to model X-ray spectroscopies.<sup>7</sup> Calculations based on the algebraic diagrammatic construction,<sup>8–10</sup> equation-of-motion<sup>11–15</sup> and linear-response<sup>16,17</sup> coupled-cluster, and multiconfigurational self-consistent-field theories<sup>18,19</sup> can now be routinely performed on small molecules. Nonetheless, the most popular approaches to model X-ray spectroscopies are those based on density functional theory (DFT).

The popularity of DFT-based methods stems from their ability to provide sufficiently accurate results for a broad range (both in complexity and size) of chemical systems at a significantly lower computational cost and broad applicability when compared to more accurate wavefunction-based methods. In this regard, LR-TDDFT,<sup>20</sup> in particular, has proven to be a powerful and versatile technique in the treatment of excited states.

In this paper, we give a short perspective from the point of view of our experiences in the development and application of Gaussian basis set based LR-TDDFT methods for X-ray spectroscopies in the NWChem computational chemistry program.<sup>21,22</sup> To this end, we focus our discussion on the computation of X-ray Near-Edge Structure (XANES), Valence-to-Core X-ray Emission (VtC-XES), and Resonant Inelastic X-ray Scattering (RIXS) spectroscopies in molecular systems within the LR-TDDFT framework. We have also tried to provide an exhaustive reference list for the interested reader covering the topics discussed.

<sup>a</sup> Department of Chemistry, The University of Memphis, Memphis, TN, 38152, USA.  
E-mail: [daniel.nascimento@memphis.edu](mailto:daniel.nascimento@memphis.edu)

<sup>b</sup> Physical and Computational Sciences Directorate, Pacific Northwest National Laboratory, Richland, Washington 99352, USA. E-mail: [niri.govind@pnl.gov](mailto:niri.govind@pnl.gov)



## 2 X-ray absorption near-edge structure

X-ray absorption edges are labelled according to the core orbitals from where the electrons are excited. XAS K-, L-, and M-edge spectra originate from photo-excitations of electrons in  $n = 1$ ,  $n = 2$ , and  $n = 3$  orbitals, respectively, where  $n$  represents the principal quantum number. In addition, spin-orbit coupling splits the degenerate orbitals with angular momentum  $l$  into  $l \pm 1/2$  manifolds. These splittings give rise to unique features that also need to be considered in the calculations.

The near edge region of the XAS is typically referred to as the near edge X-ray absorption fine structure (NEXAFS) or the X-ray absorption near edge structure (XANES). This region of the spectrum is composed of excitations from the relevant core orbitals to the bound electronic states close to the ionization potential. An illustration of the XANES process for a hypothetical octahedral transition metal complex at the K-edge is shown in the left panel of Fig. 1.

XANES carries important information about the chemical state of the atom (for example, oxidation state, coordination, bonding, *etc.*). On the other hand, the extended X-ray absorption fine structure (EXAFS) region, is composed of excitations to energies sufficient to cause ejection of a photoelectron, with subsequent scattering off nearby atoms. EXAFS yields structural information about neighboring atoms (for example, identity, distances, coordination/solvent shells, *etc.*).

From a theoretical standpoint, XANES and EXAFS are usually treated distinctly. In EXAFS, the spectral oscillations arise from modulation of X-ray absorption due to scattering of the photoelectron from nearby atoms. The essential physical quantities in EXAFS are the scattering amplitude and phase shifts, from which the spectrum is typically computed using a damped spherical photoelectron wavefunction approximation. These quantities can now be routinely computed using Green's function formalisms with localized ("muffin tin") potentials and have been very successful in modeling EXAFS spectra. Since a detailed discussion of EXAFS is beyond the scope of this paper, we refer the interested reader to comprehensive reviews on the subject.<sup>23–25</sup>

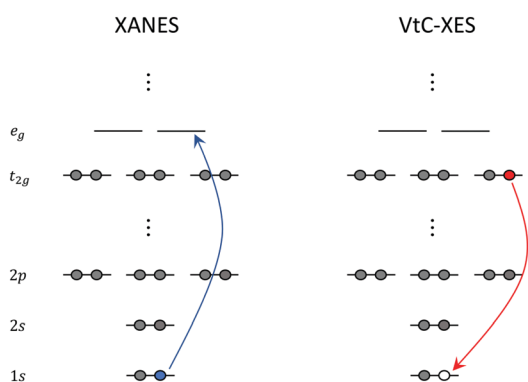


Fig. 1 Schematic representation of XANES and VtC-XES at the K-edge of a hypothetical octahedral transition metal complex.

The XANES region, on the other hand, requires an accurate electronic structure treatment of the absorbing atom and neighboring atoms bonded to it. Since core electrons move at significant fractions of the speed of light, relativistic effects have to be considered in the electronic structure descriptions. Over the years many *ab initio* methods have been developed to compute XANES at different levels of computational complexity.<sup>26,27</sup> These include methods based on density functional theory (DFT),<sup>28</sup> linear response (LR) and real-time (RT) time-dependent density functional theory (TDDFT),<sup>29–45</sup> Bethe–Salpeter equation (BSE),<sup>46–48</sup> algebraic-diagrammatic construction (ADC),<sup>49–51</sup> linear-response density cumulant theory,<sup>52</sup> coupled-cluster theory using both the complex polarization propagator<sup>53,54</sup> and equation-of-motion<sup>55–58</sup> frameworks, restricted active space (RAS) multiconfigurational methods,<sup>59–62</sup> and multireference coupled cluster methods.<sup>63</sup>

Over the past two decades, LR-TDDFT has become a computationally attractive approach for studying excited-state spectra, within the space of single excitations, in a wide range of molecular systems. Excitation energies in LR-TDDFT are obtained as solutions to the non-Hermitian eigenvalue equation or Casida matrix equations,<sup>64,65</sup>

$$\begin{pmatrix} \mathbf{A} & \mathbf{B} \\ \mathbf{B}^* & \mathbf{A}^* \end{pmatrix} \begin{pmatrix} \mathbf{X}_I \\ \mathbf{Y}_I \end{pmatrix} = \Omega_I \begin{pmatrix} 1 & 0 \\ 0 & -1 \end{pmatrix} \begin{pmatrix} \mathbf{X}_I \\ \mathbf{Y}_I \end{pmatrix} \quad (1)$$

where  $\mathbf{X}_I$ ,  $\mathbf{Y}_I$  are the solutions and  $\Omega_I$  is the excitation energy of excited-state  $I$ . The solution also yields the first-order polarization densities that can be used to compute the transition moments between the ground and excited states. Here,

$$A_{ia,jb} = (\varepsilon_a - \varepsilon_i)\delta_{ij}\delta_{ab} + (ia|jb) - c_x(ij|ab) + f_{ia,jb}^{\text{xc}} \quad (2)$$

$$B_{ia,jb} = (ia|bj) - c_x(ib|aj) + f_{ia,bj}^{\text{xc}} \quad (3)$$

$$(pq|rs) = \int d\mathbf{r} \int d\mathbf{r}' \phi_p^*(\mathbf{r})\phi_q(\mathbf{r}) \left( \frac{1}{\mathbf{r} - \mathbf{r}'} \right) \phi_r^*(\mathbf{r}')\phi_s(\mathbf{r}'), \quad (4)$$

where  $\phi_p$  is a molecular orbital with energy  $\varepsilon_p$ , and  $c_x$  represents the amount of Hartree–Fock exchange. Here, the labels  $i, j, k, l, \dots, a, b, c, d, \dots$ , and  $p, q, r, s, \dots$  denote occupied, virtual, and generic molecular orbitals, respectively.

$$f_{pq,rs}^{\text{xc}} = \int d\mathbf{r} \int d\mathbf{r}' \phi_p^*(\mathbf{r})\phi_q(\mathbf{r}) \left( \frac{\delta^2 E_{\text{xc}}[\rho]}{\delta\rho(\mathbf{r})\delta\rho(\mathbf{r}')} \Big|_{\rho=\rho_0} \right) \phi_r^*(\mathbf{r}')\phi_s(\mathbf{r}') \quad (5)$$

is the second derivative response from the exchange–correlation functional. Formally, the exact exchange–correlation kernel is a functional of the initial state and full history of the density with an unknown form. Therefore, approximations have to be used in practice. The most common approximation is to ignore the memory dependence and use the instantaneous electron density. This is also called the adiabatic approximation.<sup>20</sup> This approximation simplifies the TDDFT framework by allowing one to use extensively developed exchange–correlation functionals within ground state DFT, under the assumption that they remain valid as the many-electron density evolves in time. However, the lack of time-dependence within the adiabatic approximation, which is equivalent to a frequency-independent kernel within



linear response theory, has been linked to the lack of double excitations within TDDFT by Maitra and co-workers.<sup>66</sup>

Within the Tamm–Dancoff approximation (TDA), the above matrix equation reduces to the Hermitian equation,<sup>67</sup>

$$\mathbf{A}\mathbf{X}_I = \Omega_I\mathbf{X}_I \quad (6)$$

The TDA is formally similar to the configuration interaction singles (CIS) method with an exchange–correlation correction. Most TDDFT/TDA implementations utilize the Davidson algorithm,<sup>68</sup> which is an iterative subspace approach, to compute the lowest valence excitations or a top-down approach and other efficient algorithms.<sup>69–75</sup> Since core excitations lie very high in the excitation manifold, they are computationally expensive because the full excitation matrices have to be constructed and subsequently diagonalized, or in other words, one has to calculate a large number of roots to access the core excitations. Formally, the numerical cost of diagonalizing the full TDDFT/TDA equations scales as  $O(N^6)$ , because of the tetradic nature of the RPA matrix.<sup>76</sup> To overcome this computational issue, restricted occupied orbital space or restricted excitation window (REW) approaches, which only include the relevant core orbitals within a predefined energy window and no restrictions on the target unoccupied states, have been implemented to capture core excitations efficiently. This simple solution is valid because the core excitations are well-separated from the valence-to-valence transitions. This is similar to the core-valence separation approach.<sup>77,78</sup> Alternative approaches include the projection method that allows transitions within a specified energy range to be determined,<sup>79</sup> and the resonant converged complex polarization propagator approach.<sup>80,81</sup>

So far we have implicitly assumed the computation of K-edge XANES, which is preferred for studying light elements due to the larger core-hole lifetimes. It is also simpler to compute and interpret. On the other hand, the L-edge is preferred for transition metals and heavier elements. For instance, in transition metal complexes, the  $2p \rightarrow nd$  transitions are dipole allowed, making the L-edge XANES sensitive to partially occupied d orbitals and the bonding environment. However, computations of the L-edge XANES are more complicated due spin–orbit (SO) splitting associated with the 2p orbitals leading to the  $L_{2,3}$  XANES. The SO splitting requires at least a scalar relativistic approach with perturbative spin–orbit effects<sup>82</sup> or more rigorously, relativistic two-component (2c)<sup>36,39</sup> or four-component (4c)<sup>40,41,44</sup> LR-TDDFT treatments, where the scalar and SO effects are treated variationally, to be able to assign the spectral features at the L- and M-edges XANES accurately.

A key point in the simulation of X-ray spectroscopies is the computation of oscillator strengths, where it is important to go beyond the dipole approximation to capture the spectral features observed in experiment. Transition metal K-edge XANES is dominated by intense electric dipole allowed  $1s \rightarrow np$  transitions. However, the spectra also contain weak transitions lying at lower energies that are electric quadrupole allowed transitions to unoccupied valence d orbitals.<sup>83,84</sup> Including the electric quadrupolar contribution brings in an arbitrary dependence on the molecular origin. A widely used

approach for remedying this problem is to shift the origin to the coordinates of the absorbing atom. However, this protocol fails when there are symmetry-equivalent or several absorbing centers (for example, in multivalent transition metal clusters). Another important requirement is the Thomas–Reiche–Kuhn (TRK) sum rule, which states that the integrated oscillator strength equals the number of electrons in the system.<sup>85</sup> The TRK sum rule is satisfied only if the oscillator strengths are treated to infinite order. Any finite order treatment of the oscillator strengths does not guarantee this.<sup>86,87</sup> This suggests a more careful treatment is required. Jacob and co-workers have reported a detailed analysis and importance of the higher-order contributions to the oscillator strength.<sup>88</sup> More advanced treatments of going beyond the dipole approximation have since been developed and reported by List and co-workers.<sup>89–91</sup>

LR-TDDFT/TDA is sufficiently predictive and has been applied to a broad range of systems to compute K-edge, L-edge, and M-edge XANES<sup>29–45,84,92–103</sup> as well as transient X-ray absorption spectroscopy.<sup>104–109</sup> In Fig. 2 and 3 we show the experimental and computed K-edge XANES and  $L_3$ -edge XANES of model Fe and Ru complexes in different oxidation states. Despite this broad applicability, we emphasize that care must be taken especially in terms of the exchange–correlation functional and basis set choices, which have to be carefully assessed when performing XANES calculations. We refer the reader to

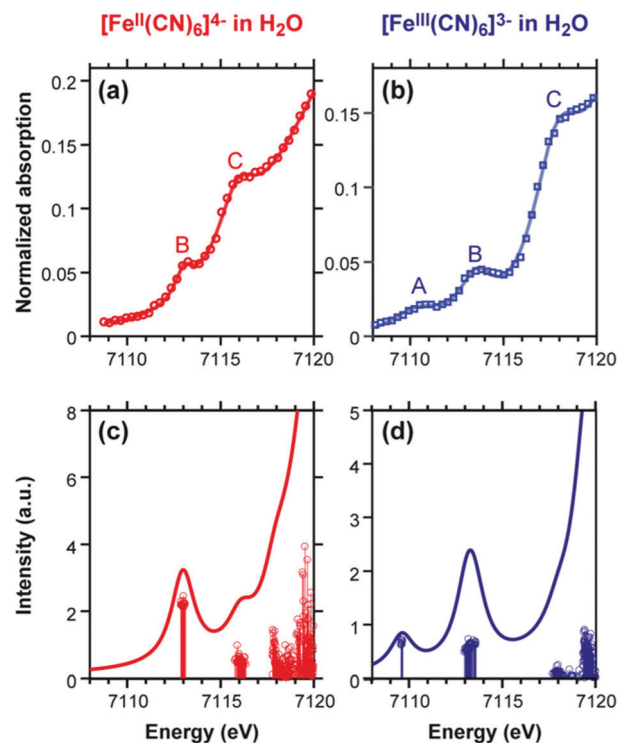
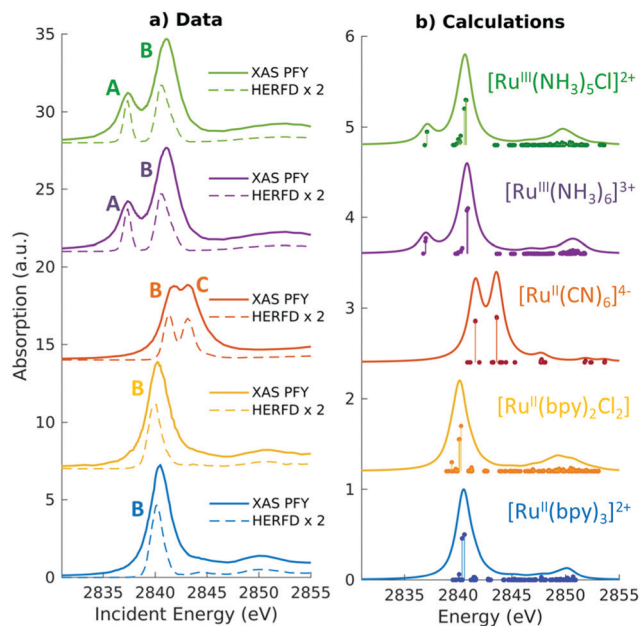


Fig. 2 Experimental (top) and simulated (bottom) Fe K-edge XANES spectra of  $[\text{Fe}^{\text{II}}(\text{CN})_6]^{4-}$  and  $[\text{Fe}^{\text{III}}(\text{CN})_6]^{3-}$  simulated results have been blue-shifted by 143.0 eV to match the experiment. The A and B features in the two complexes are quadrupolar transitions from the Fe  $1s \rightarrow 3d$  orbitals. Reproduced with permission from ref. 84. Copyright 2018 American Chemical Society.





**Fig. 3** Experimental and simulated Ru  $L_3$  edge XANES spectra of a series of Ru(II) and Ru(III) complexes with low-spin  $d^6$  and  $d^5$  configurations, respectively. The features in the two complexes correspond to dipolar transitions from the Ru  $2p \rightarrow 4d$  orbitals. A shift of 2.3 eV has been applied to the calculated spectra to match experiment. Reproduced with permission from ref. 102. Copyright 2021 Royal Society of Chemistry.

recent papers by Besley<sup>43</sup> and Jensen and co-workers<sup>110</sup> for a discussion of these topics.

### 3 Valence-to-core X-ray emission spectroscopy

Over the last several years, there has been a growing interest in X-ray emission spectroscopy (XES), and especially valence-to-core (VtC) XES,<sup>4,111</sup> which can be viewed as a complement to XANES. VtC-XES has emerged as a powerful technique for the structural characterization of transition metal complexes. Understanding the local chemical environment and electronic structure of these complexes is essential to the development of novel catalysts and materials that can be leveraged in photochemical energy conversion.

In a VtC-XES process, a core-hole is created *via* X-ray photoionization or radioactive electron capture decay<sup>112</sup> followed by the emission of a photon as electrons in higher occupied core or valence orbitals re-populate the core-hole. The resulting VtC-XES lines, which lie in the high-energy tail of the X-ray emission spectrum, thus represent the electronic transitions from valence orbitals into the empty core orbital. An illustration of the VtC-XES process for a hypothetical octahedral transition metal complex at the K-edge (where a core-hole is created in the metal  $1s$  orbital) is shown in the right panel of Fig. 1. Since the dipole selection rule forbids transitions between the metal  $d$  and  $1s$  orbitals, the weak signals that emerge from VtC-XES result from the mixing of the metal  $d$  and ligand  $s$  and  $p$  orbitals.

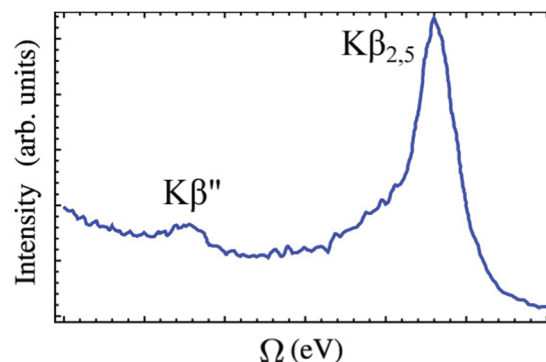


**Fig. 4** A typical VtC X-ray emission spectrum showing  $K\beta''$  and  $K\beta_{2,5}$  features (experimental spectrum of  $[Cr^{III}(NH_3)_6]^{3+}$  adapted from ref. 118). The baseline of the spectrum is not horizontal because the exponential tail of the strong  $K\beta$  mainline has not been subtracted. Reproduced with permission from ref. 119. Copyright 2015 American Chemical Society.

These orbitals play a dominant role in the chemical bonding between the metal centers and ligands. Thus, VtC-XES can provide valuable information about the nature of metal–ligand bonding.

VtC-XES features are traditionally grouped into two categories:  $K\beta''$  and  $K\beta_{2,5}$  as shown in Fig. 4. The  $K\beta''$  peaks, weak and appearing at lower energy, correspond to transitions involving the ligand  $s$  orbitals, while the  $K\beta_{2,5}$  dominant feature is assigned to transitions involving ligand  $p$  orbitals.<sup>113</sup> Thus, the splitting between the  $K\beta''$  and  $K\beta_{2,5}$  peaks is associated with the difference in binding energies between the ligand  $s$  and  $p$  orbitals. Bergmann *et al.* showed that the strength of the  $K\beta''$  peak depends exponentially on the metal–ligand distance,<sup>114</sup> and thus, provide important information for ligand characterization. The intensities of VtC-XES features can also be used to analyze the composition of valence orbitals.<sup>115–117</sup>

Over the last few years, several studies employing an independent-particle density functional theory (DFT) approach to model VtC-XES have emerged.<sup>115–118,120–125</sup> In this approach, core-hole and valence-ionized states are simply represented as single Slater determinants of ground-state Kohn–Sham orbitals, where emission energies are given by the difference in valence ( $v$ ) and core ( $c$ ) orbital energies,

$$\Delta E = \varepsilon_v - \varepsilon_c \quad (7)$$

and emission probabilities are proportional to the dipole transition moment between the respective valence and core Kohn–Sham orbitals

$$f \propto |\langle \phi_c | \hat{\mu} | \phi_v \rangle|^2. \quad (8)$$

Nonetheless, several limitations with this approach can be readily identified: the neglect of orbital relaxation due to the photon emission, the neglect of multichannel effects, and the neglect of many-body effects, to name a few.

As an alternative, the initial core hole state can be modeled within a core-hole approximation<sup>120,126–136</sup> and used as the reference for a LR-TDDFT calculation. Emission energies and transition moments are thus obtained from the solutions of the



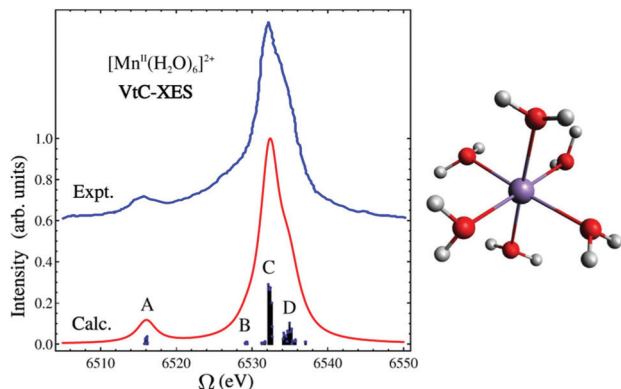


Fig. 5 Experimental and simulated VtC-XES spectra of  $[\text{Mn}^{\text{II}}(\text{H}_2\text{O})_6]^{2+}$ . Simulated results have been red-shifted by 30.4 eV to match experiment.<sup>120</sup> The molecular structure is shown on the right. Color code: O (red), Mn (purple), H (white). Reproduced with permission from ref. 119. Copyright 2015 American Chemical Society.

LR-TDDFT equations.<sup>135,136</sup> This procedure corrects for many-body and multichannel effects as it introduces orbital relaxation in the final valence-ionized states. This approach has been successfully explored by Govind and co-workers<sup>84,102,136–139</sup> and recently in machine learning models to chemically classify sulphurorganic<sup>140</sup> and organophosphorus compounds.

In this LR-TDDFT based protocol, a neutral ground state calculation is first performed, a full core-hole (FCH) ionized state is then obtained self-consistently where the 1s core orbital of the emitting center is swapped with a virtual orbital, then a LR-TDDFT<sup>141,142</sup> calculation employing the TDA<sup>143</sup> is performed with the FCH ionized state as reference. The maximum overlap constraint method is employed to prevent core hole collapse during the FCH calculation.<sup>144–146</sup> This approach is well-suited to describe emission processes with multideterminant character as seen in the spectra of the  $[\text{Mn}^{\text{II}}(\text{H}_2\text{O})_6]^{2+}$  complex (shown in Fig. 5). In Fig. 5, the B, C and D features consist of transitions from linear combinations of oxygen 2p orbitals to the Mn 1s core hole, and the A feature is composed of transitions involving the oxygen 2s orbitals. The experimental spectrum shows a strong broad peak and some weak features in the low energy region. The asymmetric shape of the strong peak indicates the existence of adjacent weak shoulders at both low and high energies in the region around the main peak. The simulated spectrum clearly captures these weak features (B and D features in Fig. 5) in good agreement with experiment.<sup>136</sup> In Fig. 6, the computed 4d  $\rightarrow$  2p VtC-XES spectra of a series of Ru(II) and Ru(III) complexes using the same method are shown and compared with experiment.<sup>102</sup>

## 4 Resonant inelastic X-ray spectroscopy

Resonant inelastic X-ray scattering (RIXS)<sup>147–149</sup> is a scattering process involving two-photons. The system is initially excited at a given X-ray absorption region accompanied by the emission of a photon of lower energy. The RIXS process results in a final excited state that cannot be accessed directly from the ground

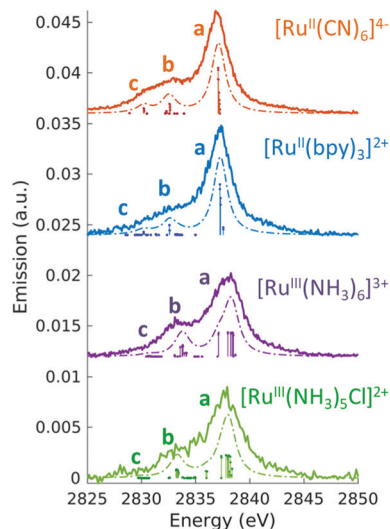


Fig. 6 Experimental (solid lines) and simulated (dashed lines) 4d  $\rightarrow$  2p VtC-XES spectra of a series of Ru(II) and Ru(III) complexes with low-spin  $d^6$  and  $d^5$  configurations, respectively. A global shift of 96.3 eV is applied to the calculated spectra. Reproduced with permission from ref. 102. Copyright 2021 Royal Society of Chemistry.

state *via* a one-photon process. Hence, RIXS maps carry important information about the electronic structure of the system that is not readily available from one-photon spectroscopies due to selection rule restrictions. A schematic representation of the RIXS process for a prototypical octahedral transition metal complex is shown in Fig. 7. Fig. 7 illustrates a scenario where the goal is to determine the crystal field splitting,  $10 Dq$ , for a low-spin  $d^6$  octahedral complex. A direct  $t_{2g} \rightarrow e_g$  transition is forbidden *via* single-photon absorption but accessible *via* a 3p4d RIXS process. In 3p4d RIXS, an electron is resonantly excited from the 3p orbitals in the metal center into the empty 4d orbitals (of  $e_g$  symmetry in the illustration above) accompanied by the repopulation of the 3p orbitals with one of the  $t_{2g}$  electrons, resulting in the  $t_{2g}^5 e_g^1$  excited state.

RIXS has been employed in the study of molecular systems in the condensed phase since its inception almost three decades ago,<sup>150</sup> nonetheless, application of RIXS in the study of molecules in the gas or solution phase only became a reality

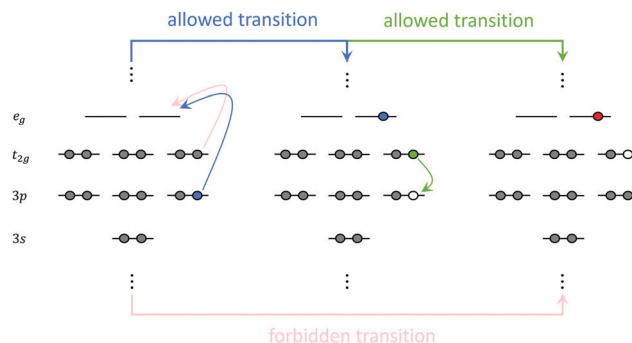


Fig. 7 Schematic representation of the RIXS process for a hypothetical octahedral transition metal complex.



in recent years.<sup>84,151–159</sup> One of the factors that restricts the applicability of RIXS in the study of gas or solution-phase molecular systems is the need for high-intensity light sources, as the concentration of absorbing atomic centers in solution is relatively low. This is not necessarily the case in condensed phases, where the abundance of absorbing atomic centers means that core-excited states can be easily accessed without the need of high-intensity light sources.<sup>160</sup> With current advances in light-source technologies and the introduction of the Linac Coherent Light Source II (LCLS-II) and European X-Ray Free-Electron Laser (European XFEL), RIXS is quickly becoming an important technique in the study of molecular systems. As RIXS experiments are rapidly becoming routine, there is an increasing demand for inexpensive electronic structure methods that are sufficiently accurate to aid in the interpretation and prediction of complicated spectral features.

In recent years, several theoretical approaches aimed at the description of RIXS spectra for molecules have been proposed. Accurate methodologies based on the damped response and equation-of-motion coupled-cluster,<sup>161–164</sup> algebraic diagrammatic construction,<sup>165</sup> multiconfigurational self-consistent field,<sup>166</sup> and configuration interaction<sup>167</sup> theories, can now be applied to small molecules with remarkable accuracy. However, wavefunction-based methods, despite their high-accuracy and black-box nature, remain too expensive to be routinely applied to large molecular systems with 100 or more electrons. Thus, simpler approaches based on density functional theory (DFT), are valuable alternatives to study large molecules, as they are significantly cheaper than wavefunction-based methods and are able to provide sufficiently accurate descriptions of spectroscopic properties.<sup>168</sup>

RIXS maps can be simulated by employing the Kramers–Heisenberg (KH) equation within the electric dipole approximation,

$$S_{\xi\xi'}(\omega', \omega) = \frac{\omega'}{\omega} \sum_f \left| \sum_n \frac{\mu_{fn}^{\xi} \mu_{n0}^{\xi'}}{\hbar\omega - E_n + i\Gamma/2} \right|^2 \times \delta(-E_f + \hbar\omega - \hbar\omega'), \quad (9)$$

where the sum runs over all the possible intermediate ( $n$ ) and final ( $f$ ) states with energies,  $E_n$  and  $E_f$ , relative to the ground state. Here,  $\Gamma$  is the lifetime broadening,  $\hbar\omega$  and  $\hbar\omega'$  represent the energies of the absorbed and emitted photons, respectively, and  $\mu_{fn}^{\xi}$  is the  $\xi$ -component of the transition dipole moment between states  $n$  and  $f$ .

The simplest way to simulate RIXS in the context of DFT calculations is to employ the independent-particle approximation as outlined in Section 3. For 3p4d RIXS (as illustrated in Fig. 7), excitation energies are simply taken as orbital energy differences, and transition moments are calculated with respect to Kohn–Sham orbitals. Such an approach is too crude as it neglects any kind of relaxation effects in the excited states, and thus, have very limited use. A viable alternative where relaxation effects is introduced in the intermediate states (but either neglected or only partially included in the emission step) has

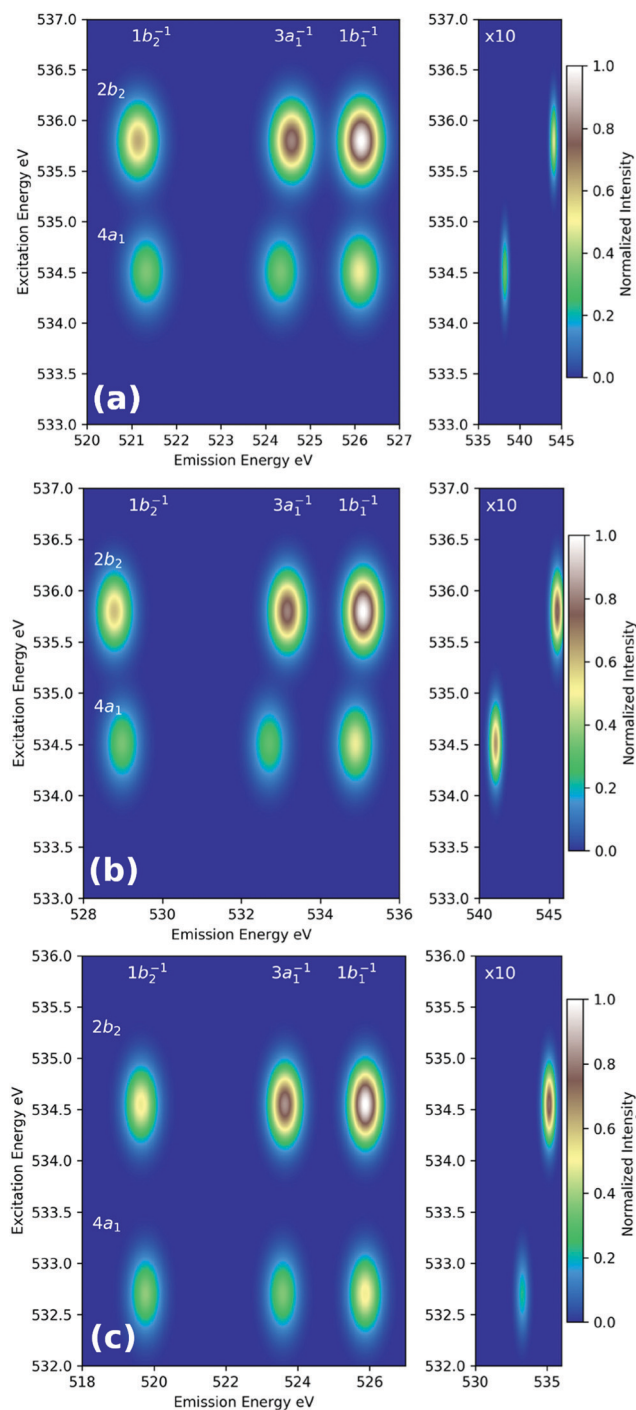


Fig. 8 Simulated RIXS maps of gas-phase water calculated with the (a) LR-TDDFT absorption/Kohn–Sham DFT emission, (b) LR-TDDFT absorption/emission, and (c) ADC(2)-x schemes for the equilibrium water structure. Adapted with permission from ref. 170. Copyright 2018 American Chemical Society.

been employed by Besley and co-workers in the RIXS study of several organic molecules.<sup>169–171</sup> In their scheme, core-excited states are calculated using a regular LR-TDDFT computation yielding accurate values for  $E_{0n}$  and  $\mu_{n0}$  whereas  $E_{fn}$  and  $\mu_{fn}$  are either determined *via* the independent-particle approximation, or by performing another LR-TDDFT computation with the



core-excited determinant as a reference. Both of these schemes yield surprisingly accurate RIXS spectra when compared with high-level second-order algebraic diagrammatic [ADC(2)-x] calculations (as illustrated in Fig. 8) or experiment.<sup>169</sup> Although the schemes employed by Beasley and co-workers can be successfully employed for small organic molecules, it can become problematic as the level of correlation of the final excited states become significant, or when many intermediate excited states participate in the RIXS process. Under these circumstances, the independent-particle model for the emission process is insufficient, and the choice of a single intermediate excited state reference becomes ambiguous and a manifold of intermediate and final states must be considered.

A consistent treatment of relaxation in both intermediate and final states can be achieved *via* a quadratic-response (QR) TDDFT treatment. In the QR-TDDFT framework, excited-state transition densities have the form

$$\delta n_{IJ}^{\text{QR}} = \delta n_{0I}^{(1)} \delta n_{0J}^{(1)} + \delta n_{IJ}^{(2)}, \quad (10)$$

where  $\delta n_{0I}^{(1)}$  is the first-order transition density obtained as the solutions of the LR-TDDFT equations,

$$\delta n_{0I}^{(1)} = \begin{pmatrix} \mathbf{X}_I \\ \mathbf{Y}_I \end{pmatrix} \quad (11)$$

and  $\delta n_{IJ}^{(2)}$  is the second-order relaxation correction obtained from QR-TDDFT. However, Dalgaard<sup>172</sup> and later Parker and co-workers<sup>173,174</sup> demonstrated that the QR equations for an approximate theory, such as TDDFT, have spurious poles whenever the transition energy between two excited states matches the excitation energy of any other state. These spurious poles can overestimate the second-order relaxation correction, and thus, must be used with caution. Additionally, due to the significant additional computational cost of QR-TDDFT, these calculations are typically limited to smaller excitation subspaces.<sup>175</sup> For instance, in systems with high density of states, each QR-TDDFT excitation must be solved individually, which can quickly become prohibitive if a complete or broad energy span spectrum is needed. For the RIXS calculations shown in Fig. 9,  $\sim O(10^3)$  valence states were coupled with  $\sim O(10^2)$  core states.

Alternatively, one can completely neglect the second-order relaxation correction and build excited-state transition densities directly from the first-order amplitudes obtained from a LR-TDDFT calculation. In this approach, two orthogonal sets of excited states (intermediate and final) are computed within a restricted subspace, and transition dipole moments are calculated as

$$\mu_{IJ} = \sum_{ijab} (X_{ai}^I X_{bj}^J - Y_{ai}^I Y_{bj}^J) (\mu_{ab} \delta_{ij} - \delta_{ab} \mu_{ji}), \quad (12)$$

where  $\mu_{pq}$  is the matrix representation of the dipole operator in the molecular orbital basis. This simplified approach is equivalent to the pseudo-wavefunction formulation of LR-TDDFT (PWF-TDDFT) proposed originally in the context of derivative couplings between Hartree-Fock excited states<sup>176</sup> and spin-flip TDDFT states,<sup>177</sup> then generalized to LR-TDDFT states.<sup>178,179</sup> Zhang and Herbert demonstrated that there is no distinction between derivative couplings obtained from quadratic-response and those obtained from a

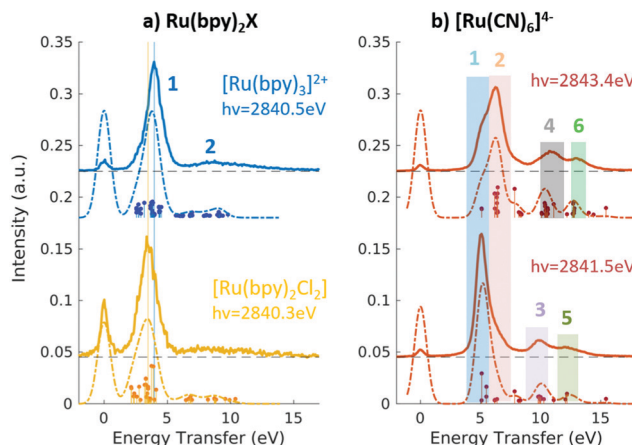


Fig. 9 Experimental (solid lines) and theoretical (dashed lines) 2p4d RIXS spectra of (a)  $[\text{Ru}^{\text{II}}(\text{bpy})_3]^{2+}$  (top) and  $[\text{Ru}^{\text{II}}(\text{bpy})_2\text{Cl}_2]$  (bottom) measured with incident X-ray energy resonant with the  $2p \rightarrow e_g$  transition as a function of energy transfer. (b)  $[\text{Ru}^{\text{II}}(\text{CN})_6]^{4-}$  measured with incident X-ray energy resonant with the  $2p \rightarrow e_g$  transition (bottom) and resonant with the  $2p \rightarrow \pi^*$  transition (top). Reproduced with permission from ref. 159. Copyright 2021 Royal Society of Chemistry.

spin-flip TDDFT pseudo-wavefunction, whereas a spin-conserving TDDFT pseudo-wavefunction does yield different couplings.<sup>180</sup>

In the context of light-matter interactions, Sheng and co-workers demonstrated that the (spin-conserving) PWF-TDDFT framework may be used to simulate excited-state absorption spectra with errors in the order of 0.07 eV with a suitable choice of exchange-correlation functional.<sup>181</sup> Vaz da Cruz and co-workers showed that PWF-TDDFT can also be applied in the simulation of RIXS spectra of organic molecules at the K-edge of light elements.<sup>182</sup> In a more recent study, Nascimento and co-workers successfully employed the PWF-TDDFT approach to simulate 2p4d RIXS of representative ruthenium complexes,<sup>183</sup> followed by a joint theoretical and experimental investigation to understand and characterize the ground and excited valence states of Ru complexes<sup>159</sup> (as illustrated in Fig. 9). Fig. 9 shows the experimental and theoretical spectra of  $[\text{Ru}^{\text{II}}(\text{bpy})_3]^{2+}$ ,  $[\text{Ru}^{\text{II}}(\text{bpy})_2\text{Cl}_2]$  and  $[\text{Ru}^{\text{II}}(\text{CN})_6]^{4-}$  under different conditions. The calculated spectra is in excellent agreement with experiment and is able to reproduce all experimental features with relative transfer energies predicted to within 0.6 eV of accuracy.

## 5 Summary and outlook

With the rapid growth of experimental X-ray spectroscopy studies, there is a simultaneous need for predictive and computationally cost-effective theoretical approaches. Spectroscopy simulations are key to disentangling spectral features and for a detailed understanding of the observed signals. Great strides have been made in the development of *ab initio* wavefunction-based methods for the simulation of X-ray spectroscopies over the last few years. Nevertheless, low-order DFT-based methods, like LR/RT-TDDFT, are still very useful. Their ability to provide sufficient accuracy for a broad range of large chemical systems in realistic environments at a significantly lower computational



cost makes these low cost methods very appealing. In this brief review, we have highlighted the utility of LR-TDDFT based approaches to tackle XANES, VtC-XES, and RIXS to analyse and interpret experimental data. However, TDDFT is not a panacea and many open questions remain and new theoretical developments are needed.<sup>184,185</sup> As we have emphasized earlier, care must be taken especially in terms of the exchange–correlation functional and basis set choices, which have to be carefully assessed when performing excited-state computations in general including core-level spectra. Other areas of development include simulations of non-linear X-ray spectroscopic signals,<sup>186</sup> transient spectroscopies<sup>187</sup> including dynamics, real-time domain simulations, and TDDFT coupled to strong fields.<sup>42</sup> Additionally, developments in applied mathematics are also needed for efficient solvers for large systems.

## Author contributions

D. R. N. and N. G. jointly wrote the article.

## Conflicts of interest

There are no conflicts to declare.

## Acknowledgements

This work was supported by the U.S. Department of Energy, Office of Science, Office of Basic Energy Sciences, Chemical Sciences, Geosciences and Biosciences Division under Award No. KC-030105172685 (D. R. N., N. G.). D. R. N. acknowledges support from the University of Memphis. This research benefited from computational resources provided by EMSL, a DOE Office of Science User Facility sponsored by the Office of Biological and Environmental Research and located at PNNL. PNNL is operated by Battelle Memorial Institute for the United States Department of Energy under DOE Contract No. DE-AC05-76RL1830. This research also used resources of the National Energy Research Scientific Computing Center (NERSC), a U.S. Department of Energy Office of Science User Facility operated under Contract No. DE-AC02-05CH11231.

## Notes and references

- 1 F. De Groot, *Chem. Rev.*, 2001, **101**, 1779–1808.
- 2 J. Stöhr, *NEXAFS Spectroscopy*, Springer-Verlag, 2003.
- 3 F. De Groot and A. Kotani, *Core Level Spectroscopy of Solids*, CRC Press, 2008.
- 4 M. Bauer, *Phys. Chem. Chem. Phys.*, 2014, **16**, 13827–13837.
- 5 R. Schoenlein, T. Elsaesser, K. Holldack, Z. Huang, H. Kapteyn, M. Murnane and M. Woerner, *Philos. Trans. R. Soc., A*, 2019, **377**, 20180384.
- 6 G. Seidler, D. Mortensen, A. Remesnik, J. Pacold, N. Ball, N. Barry, M. Styczinski and O. Hoidn, *Rev. Sci. Instrum.*, 2014, **85**, 113906.
- 7 F. M. de Groot, H. Elnaggar, F. Frati, R.-P. Wang, M. U. Delgado-Jaime, M. van Veenendaal, J. Fernandez-Rodriguez, M. W. Haverkort, R. J. Green and G. van der Laan, *et al.*, *J. Electron Spectrosc. Relat. Phenom.*, 2021, **249**, 147061.
- 8 A. Trofimov, T. Moskovskaya, E. Gromov, N. Vitkovskaya and J. Schirmer, *J. Struct. Chem.*, 2000, **41**, 483–494.
- 9 J. Wenzel, M. Wormit and A. Dreuw, *J. Comput. Chem.*, 2014, **35**, 1900–1915.
- 10 J. Wenzel, M. Wormit and A. Dreuw, *J. Chem. Theory Comput.*, 2014, **10**, 4583–4598.
- 11 B. Peng, P. J. LeStrange, J. J. Goings, M. Caricato and X. Li, *J. Chem. Theory Comput.*, 2015, **11**, 4146–4153.
- 12 D. R. Nascimento and A. E. DePrince III, *J. Phys. Chem. Lett.*, 2017, **8**, 2951–2957.
- 13 M. L. Vidal, X. Feng, E. Epifanovsky, A. I. Krylov and S. Coriani, *J. Chem. Theory Comput.*, 2019, **15**, 3117–3133.
- 14 M. L. Vidal, A. I. Krylov and S. Coriani, *Phys. Chem. Chem. Phys.*, 2020, **22**, 2693–2703.
- 15 M. L. Vidal, P. Pokhilkov, A. I. Krylov and S. Coriani, *J. Phys. Chem. Lett.*, 2020, **11**, 8314–8321.
- 16 S. Coriani and H. Koch, *J. Chem. Phys.*, 2015, **143**, 181103.
- 17 R. Faber and S. Coriani, *J. Chem. Theory Comput.*, 2018, **15**, 520–528.
- 18 R. V. Pinjari, M. G. Delcey, M. Guo, M. Odelius and M. Lundberg, *J. Chem. Phys.*, 2014, **141**, 124116.
- 19 B. Helmich-Paris, *Int. J. Quantum Chem.*, 2021, **121**, e26559.
- 20 C. A. Ullrich, *Time-Dependent Density-Functional Theory: Concepts and Applications*, Oxford University Press, 2011.
- 21 M. Valiev, E. J. Bylaska, N. Govind, K. Kowalski, T. P. Straatsma, H. J. Van Dam, D. Wang, J. Nieplocha, E. Apra, T. L. Windus and W. A. De Jong, *Comput. Phys. Commun.*, 2010, **181**, 1477–1489.
- 22 E. Apra, E. J. Bylaska, W. A. De Jong, N. Govind, K. Kowalski, T. P. Straatsma, M. Valiev, H. J. van Dam, Y. Alexeev and J. Anchell, *et al.*, *J. Chem. Phys.*, 2020, **152**, 184102.
- 23 J. J. Rehr and R. C. Albers, *Rev. Mod. Phys.*, 2000, **72**, 621–654.
- 24 J. J. Rehr, J. J. Kas, M. P. Prange, A. P. Sorini, Y. Takimoto and F. Vila, *C. R. Phys.*, 2009, **10**, 548–559.
- 25 J. J. Rehr, J. J. Kas, F. D. Vila, M. P. Prange and K. Jorissen, *Phys. Chem. Chem. Phys.*, 2010, **12**, 5503–5513.
- 26 P. Norman and A. Dreuw, *Chem. Rev.*, 2018, **118**, 7208–7248.
- 27 J. M. Kasper, T. F. Stetina, A. J. Jenkins and X. Li, *Chem. Phys. Rev.*, 2020, **1**, 011304.
- 28 N. A. Besley, *Acc. Chem. Res.*, 2020, **53**, 1306–1315.
- 29 M. Stener, G. Fronzoni and M. de Simone, *Chem. Phys. Lett.*, 2003, **373**, 115–123.
- 30 K. Ray, S. DeBeer George, E. I. Solomon, K. Wieghardt and F. Neese, *Chem. – Eur. J.*, 2007, **13**, 2783–2797, DOI: [10.1002/chem.200601425](https://doi.org/10.1002/chem.200601425).
- 31 N. A. Besley and F. A. Asmuruf, *Phys. Chem. Chem. Phys.*, 2010, **12**, 12024–12039.
- 32 W. Liang, S. A. Fischer, M. J. Frisch and X. Li, *J. Chem. Theory Comput.*, 2011, **7**, 3540–3547.





- 33 K. Lopata, B. E. Van Kuiken, M. Khalil and N. Govind, *J. Chem. Theory Comput.*, 2012, **8**, 3284–3292.
- 34 B. Peng, P. J. LeStrange, J. J. Goings, M. Caricato and X. Li, *J. Chem. Theory Comput.*, 2015, **11**, 4146–4153.
- 35 R. Van Beeumen, D. B. Williams-Young, J. M. Kasper, C. Yang, E. G. Ng and X. Li, *J. Chem. Theory Comput.*, 2017, **13**, 4950–4961.
- 36 G. Fronzoni, M. Stener, P. Decleva, M. D. Simone, M. Coreno, P. Franceschi, C. Furlani and K. Prince, *J. Phys. Chem. A*, 2009, **113**, 2914–2925.
- 37 M. Kadek, L. Konecny, B. Gao, M. Repisky and K. Ruud, *Phys. Chem. Chem. Phys.*, 2015, **17**, 22566–22570.
- 38 M. Repisky, L. Konecny, M. Kadek, S. Komorovsky, O. L. Malkin, V. G. Malkin and K. Ruud, *J. Chem. Theory Comput.*, 2015, **11**, 980–991.
- 39 T. F. Stetina, J. M. Kasper and X. Li, *J. Chem. Phys.*, 2019, **150**, 234103.
- 40 C. South, A. Shee, D. Mukherjee, A. K. Wilson and T. Saue, *Phys. Chem. Chem. Phys.*, 2016, **18**, 21010–21023.
- 41 T. Fransson, D. Burdakova and P. Norman, *Phys. Chem. Chem. Phys.*, 2016, **18**, 13591–13603.
- 42 X. Li, N. Govind, C. Isborn, A. E. DePrince and K. Lopata, *Chem. Rev.*, 2020, **120**, 9951–9993.
- 43 N. A. Besley, *Wiley Interdiscip. Rev.: Comput. Mol. Sci.*, 2021, **11**, e1527.
- 44 L. Konecny, J. Vicha, S. Komorovsky, K. Ruud and M. Repisky, *Inorg. Chem.*, 2021, **61**, 830–846.
- 45 A. Bussy and J. Hutter, *Phys. Chem. Chem. Phys.*, 2021, **23**, 4736–4746.
- 46 G. Onida, L. Reining and A. Rubio, *Rev. Mod. Phys.*, 2002, **74**, 601.
- 47 J. Vinson, J. Rehr, J. Kas and E. Shirley, *Phys. Rev. B: Condens. Matter Mater. Phys.*, 2011, **83**, 115106.
- 48 Y. Yao, D. Golze, P. Rinke, V. Blum and Y. Kanai, *J. Chem. Theory Comput.*, 2022, **18**, 1569–1583, DOI: [10.1021/acs.jctc.1c01180](https://doi.org/10.1021/acs.jctc.1c01180).
- 49 J. Wenzel, M. Wormit and A. Dreuw, *J. Comput. Chem.*, 2014, **35**, 1900–1915, DOI: [10.1002/jcc.23703](https://doi.org/10.1002/jcc.23703).
- 50 J. Wenzel, M. Wormit and A. Dreuw, *J. Chem. Theory Comput.*, 2014, **10**, 4583–4598.
- 51 J. Wenzel, A. Holzer, M. Wormit and A. Dreuw, *J. Chem. Phys.*, 2015, **142**, 214104.
- 52 R. Peng, A. V. Copan and A. Y. Sokolov, *J. Phys. Chem. A*, 2019, **123**, 1840–1850.
- 53 S. Coriani, O. Christiansen, T. Fransson and P. Norman, *Phys. Rev. A*, 2012, **85**, 022507.
- 54 T. Fransson, S. Coriani, O. Christiansen and P. Norman, *J. Chem. Phys.*, 2013, **138**, 124311.
- 55 D. R. Nascimento and A. E. DePrince III, *J. Phys. Chem. Lett.*, 2017, **8**, 2951–2957.
- 56 J. Liu, D. Matthews, S. Coriani and L. Cheng, *J. Chem. Theory Comput.*, 2019, **15**, 1642–1651.
- 57 Y. C. Park, A. Perera and R. J. Bartlett, *J. Chem. Phys.*, 2021, **155**, 094103.
- 58 D. A. Matthews, *Mol. Phys.*, 2020, **118**, e1771448.
- 59 I. Josefsson, K. Kunnus, S. Schreck, A. Föhlisch, F. de Groot, P. Wernet and M. Odellius, *J. Phys. Chem. Lett.*, 2012, **3**, 3565–3570.
- 60 R. V. Pinjari, M. G. Delcey, M. Guo, M. Odellius and M. Lundberg, *J. Chem. Phys.*, 2014, **141**, 124116.
- 61 M. Roemelt and F. Neese, *J. Phys. Chem. A*, 2013, **117**, 3069–3083.
- 62 M. Roemelt, D. Maganas, S. DeBeer and F. Neese, *J. Chem. Phys.*, 2013, **138**, 204101.
- 63 J. Brabec, K. Bhaskaran-Nair, N. Govind, J. Pittner and K. Kowalski, *J. Chem. Phys.*, 2012, **137**, 171101.
- 64 M. E. Casida, *Time-Dependent Density-functional Response Theory for Molecules*, World Scientific, 1995, pp. 155–193.
- 65 C. A. Ullrich, *Time-Dependent Density-Functional Theory: Concepts and Applications*, OUP, Oxford, 2011.
- 66 N. T. Maitra, F. Zhang, R. J. Cave and K. Burke, *J. Chem. Phys.*, 2004, **120**, 5932–5937.
- 67 S. Hirata and M. Head-Gordon, *Chem. Phys. Lett.*, 1999, **314**, 291–299.
- 68 E. R. Davidson, *J. Comput. Phys.*, 1975, **17**, 87–94.
- 69 J. Brabec, L. Lin, M. Shao, N. Govind, C. Yang, Y. Saad and E. G. Ng, *J. Chem. Theory Comput.*, 2015, **11**, 5197–5208.
- 70 F. Furche, B. T. Krull, B. D. Nguyen and J. Kwon, *J. Chem. Phys.*, 2016, **144**, 174105.
- 71 E. Vecharynski, J. Brabec, M. Shao, N. Govind and C. Yang, *Comput. Phys. Commun.*, 2017, **221**, 42–52.
- 72 C. Huang, W. Liu, Y. Xiao and M. R. Hoffmann, *J. Comput. Chem.*, 2017, **38**, 2481–2499.
- 73 J. M. Kasper, D. B. Williams-Young, E. Vecharynski, C. Yang and X. Li, *J. Chem. Theory Comput.*, 2018, **14**, 2034–2041.
- 74 C. Huang and W. Liu, *J. Comput. Chem.*, 2019, **40**, 1023–1037.
- 75 S. Komorovsky, P. J. Cherry and M. Repisky, *J. Chem. Phys.*, 2019, **151**, 184111.
- 76 S. Tretiak, C. M. Isborn, A. M. Niklasson and M. Challacombe, *J. Chem. Phys.*, 2009, **130**, 054111.
- 77 L. S. Cederbaum, W. Domcke and J. Schirmer, *Phys. Rev. A: At., Mol., Opt. Phys.*, 1980, **22**, 206.
- 78 M. F. Herbst and T. Fransson, *J. Chem. Phys.*, 2020, **153**, 054114.
- 79 T. Tsuchimochi, M. Kobayashi, A. Nakata, Y. Imamura and H. Nakai, *J. Comput. Chem.*, 2008, **29**, 2311–2316.
- 80 U. Ekström and P. Norman, *Phys. Rev. A: At., Mol., Opt. Phys.*, 2006, **74**, 042722.
- 81 U. Ekström, P. Norman, V. Carravetta and H. Ågren, *Phys. Rev. Lett.*, 2006, **97**, 143001.
- 82 M. Roemelt, D. Maganas, S. DeBeer and F. Neese, *J. Chem. Phys.*, 2013, **138**, 204101.
- 83 S. D. George, T. Petrenko and F. Neese, *Inorg. Chim. Acta*, 2008, **361**, 965–972.
- 84 M. Ross, A. Andersen, Z. W. Fox, Y. Zhang, K. Hong, J.-H. Lee, A. Cordones, A. M. March, G. Doumy, S. H. Southworth, M. A. Marcus, R. W. Schoenlein, S. Mukamel, N. Govind and M. Khalil, *J. Phys. Chem. B*, 2018, **122**, 5075–5086.
- 85 H. A. Albrecht and E. E. Salpeter, *Quantum Mechanics for One-and Two-electron Atoms*, Springer, 1957.
- 86 P. J. LeStrange, F. Egidi and X. Li, *J. Chem. Phys.*, 2015, **143**, 234103.



- 87 L. Zheng, N. F. Polizzi, A. R. Dave, A. Migliore and D. N. Beratan, *J. Phys. Chem. A*, 2016, **120**, 1933–1943.
- 88 S. Bernadotte, A. J. Atkins and C. R. Jacob, *J. Chem. Phys.*, 2012, **137**, 204106.
- 89 N. H. List, J. Kauczor, T. Saue, H. J. A. Jensen and P. Norman, *J. Chem. Phys.*, 2015, **142**, 244111.
- 90 N. H. List, T. Saue and P. Norman, *Mol. Phys.*, 2017, **115**, 63–74.
- 91 N. H. List, T. R. L. Melin, M. van Horn and T. Saue, *J. Chem. Phys.*, 2020, **152**, 184110.
- 92 B. E. Van Kuiken, M. Valiev, S. L. Daifuku, C. Bannan, M. L. Strader, H. Cho, N. Huse, R. W. Schoenlein, N. Govind and M. Khalil, *J. Phys. Chem. A*, 2013, **117**, 4444–4454.
- 93 A. Vjunov, J. L. Fulton, T. Huthwelker, S. Pin, D. Mei, G. K. Schenter, N. Govind, D. M. Camaioni, J. Z. Hu and J. A. Lercher, *J. Am. Chem. Soc.*, 2014, **136**, 8296–8306.
- 94 J. L. Fulton, N. Govind, T. Huthwelker, E. J. Bylaska, A. Vjunov, S. Pin and T. D. Smurthwaite, *J. Phys. Chem. B*, 2015, **119**, 8380–8388.
- 95 N. Govind and W. A. D. Jong, *Thom H. Dunning, Jr.*, Springer, 2015, pp. 247–253.
- 96 M. Vijayakumar, N. Govind, E. Walter, S. D. Burton, A. Shukla, A. Devaraj, J. Xiao, J. Liu, C. Wang and A. Karim, *et al.*, *Phys. Chem. Chem. Phys.*, 2014, **16**, 10923–10932.
- 97 K. Henzler, E. O. Fetisov, M. Galib, M. D. Baer, B. A. Legg, C. Borca, J. M. Xto, S. Pin, J. L. Fulton and G. K. Schenter, *et al.*, *Sci. Adv.*, 2018, **4**, eaao6283.
- 98 M. Galib, G. Schenter, C. Mundy, N. Govind and J. Fulton, *J. Chem. Phys.*, 2018, **149**, 124503.
- 99 A. Andersen, N. N. Rajput, K. S. Han, H. Pan, N. Govind, K. A. Persson, K. T. Mueller and V. Murugesan, *Chem. Mater.*, 2019, **31**, 2308–2319.
- 100 A. Vjunov, M. Wang, N. Govind, T. Huthwelker, H. Shi, D. Mei, J. L. Fulton and J. A. Lercher, *Chem. Mater.*, 2017, **29**, 9030–9042.
- 101 V. Murugesan, J. S. Cho, N. Govind, A. Andersen, M. J. Olszta, K. S. Han, G. Li, H. Lee, D. M. Reed and V. L. Sprenkle, *et al.*, *ACS Appl. Energy Mater.*, 2019, **2**, 1832–1843.
- 102 E. Biasin, D. R. Nascimento, B. I. Poulter, B. Abraham, K. Kunnus, A. T. Garcia-Esparza, S. H. Nowak, T. Kroll, R. W. Schoenlein, R. Alonso-Mori, M. Khalil, N. Govind and D. Sokaras, *Chem. Sci.*, 2021, 3713–3725, DOI: [10.1039/D0SC06227H](https://doi.org/10.1039/D0SC06227H).
- 103 D. Boglajenko, A. Andersen, S. M. Heald, T. Varga, D. R. Mortensen, S. Tetef, G. T. Seidler, N. Govind and T. G. Levitskaia, *J. Alloys Compd.*, 2022, **897**, 162629.
- 104 A. M. March, G. Doumy, A. Andersen, A. Al Haddad, Y. Kumagai, M.-F. Tu, J. Bang, C. Bostedt, J. Uhlig and D. R. Nascimento, *et al.*, *J. Chem. Phys.*, 2019, **151**, 144306.
- 105 D. R. Nascimento, Y. Zhang, U. Bergmann and N. Govind, *J. Phys. Chem. Lett.*, 2020, **11**, 556–561.
- 106 A. S. Folorunso, A. Bruner, F. Mauger, K. A. Hamer, S. Hernandez, R. R. Jones, L. F. DiMauro, M. B. Gaarde, K. J. Schafer and K. Lopata, *Phys. Rev. Lett.*, 2021, **126**, 133002.
- 107 C. E. Liekhus-Schmaltz, P. J. Ho, R. B. Weakly, A. Aquila, R. W. Schoenlein, M. Khalil and N. Govind, *J. Chem. Phys.*, 2021, **154**, 214107.
- 108 C. M. Loe, C. Liekhus-Schmaltz, N. Govind and M. Khalil, *J. Phys. Chem. Lett.*, 2021, **12**, 9840–9847.
- 109 C. Liekhus-Schmaltz, Z. W. Fox, A. Andersen, K. S. Kjaer, R. Alonso-Mori, E. Biasin, J. Carlstad, M. Chollet, J. D. Gaynor and J. M. Glowina, *et al.*, *J. Phys. Chem. Lett.*, 2022, **13**, 378–386.
- 110 M. A. Ambrose and F. Jensen, *J. Chem. Theory Comput.*, 2018, **15**, 325–337.
- 111 E. Gallo and P. Glatzel, *Adv. Mater.*, 2014, **26**, 7730–7746.
- 112 P. Glatzel and U. Bergmann, *Coord. Chem. Rev.*, 2005, **249**, 65–95.
- 113 P. E. Best, *J. Chem. Phys.*, 1966, **44**, 3248–3253.
- 114 U. Bergmann, C. R. Horne, T. J. Collins, J. Workman and S. P. Cramer, *Chem. Phys. Lett.*, 1999, **302**, 119–124.
- 115 N. Lee, T. Petrenko, U. Bergmann, F. Neese and S. DeBeer, *J. Am. Chem. Soc.*, 2010, **132**, 9715–9727.
- 116 M. A. Beckwith, M. Roemelt, M.-N. Collomb, C. DuBoc, T.-C. Weng, U. Bergmann, P. Glatzel, F. Neese and S. DeBeer, *Inorg. Chem.*, 2011, **50**, 8397–8409.
- 117 K. M. Lancaster, K. D. Finkelstein and S. DeBeer, *Inorg. Chem.*, 2011, **50**, 6767–6774.
- 118 S. N. MacMillan, R. C. Walroth, D. M. Perry, T. J. Morsing and K. M. Lancaster, *Inorg. Chem.*, 2015, **54**, 205–214.
- 119 Y. Zhang, S. Mukamel, M. Khalil and N. Govind, *J. Chem. Theory Comput.*, 2015, **11**, 5804–5809.
- 120 G. Smolentsev, A. V. Soldatov, J. Messinger, K. Merz, T. Weyhermüller, U. Bergmann, Y. Pushkar, J. Yano, V. K. Yachandra and P. Glatzel, *J. Am. Chem. Soc.*, 2009, **131**, 13161–13167.
- 121 J. C. Swarbrick, Y. Kvashnin, K. Schulte, K. Seenivasan, C. Lamberti and P. Glatzel, *Inorg. Chem.*, 2010, **49**, 8323–8332.
- 122 E. R. Hall, C. J. Pollock, J. Bendix, T. J. Collins, P. Glatzel and S. DeBeer, *J. Am. Chem. Soc.*, 2014, **136**, 10076–10084.
- 123 A. M. March, T. A. Assefa, C. Bressler, G. Doumy, A. Galler, W. Gawelda, E. P. Kanter, Z. Németh, M. Pápai, S. H. Southworth, L. Young and G. Vankó, *J. Phys. Chem. C*, 2015, **119**, 14571–14578.
- 124 M. Qureshi, S. H. Nowak, L. I. Vogt, J. J. Cotelesage, N. V. Dolgova, S. Sharifi, T. Kroll, D. Nordlund, R. Alonso-Mori and T.-C. Weng, *et al.*, *Phys. Chem. Chem. Phys.*, 2021, **23**, 4500–4508.
- 125 N. Levin, S. Peredkov, T. Weyhermüller, O. Rüdiger, N. B. Pereira, D. Grötzsch, A. Kalinko and S. DeBeer, *Inorg. Chem.*, 2020, **59**, 8272–8283.
- 126 P. Nozières and C. T. de Dominicis, *Phys. Rev.*, 1969, **178**, 1097–1107.
- 127 W. H. E. Schwarz and R. J. Buenker, *Chem. Phys.*, 1976, **13**, 153–160.
- 128 Y. Zhang, W. Hua, K. Bennett and S. Mukamel, *Density-Functional Methods for Excited States*, Springer Science + Business Media, 2015, vol. 368, pp. 273–345.
- 129 W. J. Hunt and W. A. Goddard, *Chem. Phys. Lett.*, 1969, **3**, 414–418.



- 130 H. Ågren, V. Carravetta, O. Vahtras and L. G. Pettersson, *Chem. Phys. Lett.*, 1994, **222**, 75–81.
- 131 H. Åren, V. Carravetta, O. Vahtras and L. G. M. Pettersson, *Theor. Chem. Acc.*, 1997, **97**, 14–40.
- 132 M. Stener, A. Lisini and P. Decleva, *Chem. Phys.*, 1995, **191**, 141–154.
- 133 L. Triguero, L. G. M. Pettersson and H. Ågren, *Phys. Rev. B: Condens. Matter Mater. Phys.*, 1998, **58**, 8097–8110.
- 134 D. Prendergast and G. Galli, *Phys. Rev. Lett.*, 2006, **96**, 215502.
- 135 J. D. Wadey and N. A. Besley, *J. Chem. Theory Comput.*, 2014, **10**, 4557–4564.
- 136 Y. Zhang, S. Mukamel, M. Khalil and N. Govind, *J. Chem. Theory Comput.*, 2015, **11**, 5804–5809.
- 137 D. Mortensen, G. Seidler, J. J. Kas, N. Govind, C. P. Schwartz, S. Pemmaraju and D. G. Prendergast, *Phys. Rev. B*, 2017, **96**, 125136.
- 138 E. P. Jahrman, W. M. Holden, N. Govind, J. J. Kas, J. Rana, L. F. Piper, C. Siu, M. S. Whittingham, T. T. Fister and G. T. Seidler, *J. Mater. Chem. A*, 2020, **8**, 16332–16344.
- 139 W. Holden, E. Jahrman, N. Govind and G. Seidler, *J. Phys. Chem. A*, 2020, **124**, 5415–5434.
- 140 S. Tetef, N. Govind and G. T. Seidler, *Phys. Chem. Chem. Phys.*, 2021, **23**, 23586–23601.
- 141 M. E. Casida, *Recent Advances in Density Functional Methods (Part I)*, World Scientific, 1995, ch. 5, vol. 1, pp. 155–192.
- 142 R. E. Stratmann, G. E. Scuseria and M. J. Frisch, *J. Chem. Phys.*, 1998, **109**, 8218–8224.
- 143 S. Hirata and M. Head-Gordon, *Chem. Phys. Lett.*, 1999, **302**, 375–382.
- 144 P. G. Lykos and H. N. Schmeising, *J. Chem. Phys.*, 1961, **35**, 288–293.
- 145 H. F. King, R. E. Stanton, H. Kim, R. E. Wyatt and R. G. Parr, *J. Chem. Phys.*, 1967, **47**, 1936–1941.
- 146 A. T. B. Gilbert, N. A. Besley and P. M. W. Gill, *J. Phys. Chem. A*, 2008, **112**, 13164–13171.
- 147 F. Gel'mukhanov and H. Ågren, *Phys. Rep.*, 1999, **312**, 87–330.
- 148 F. de Groot, *Chem. Rev.*, 2001, **101**, 1779–1808.
- 149 L. J. P. Ament, M. van Veenendaal, T. P. Devereaux, J. P. Hill and J. van den Brink, *Rev. Mod. Phys.*, 2011, **83**, 705–767.
- 150 E. D. Isaacs and P. Platzman, *Phys. Today*, 1996, **49**, 40–45.
- 151 F. Hennies, A. Pietzsch, M. Berglund, A. Föhlisch, T. Schmitt, V. Strocov, H. O. Karlsson, J. Andersson and J.-E. Rubensson, *Phys. Rev. Lett.*, 2010, **104**, 193002.
- 152 J. Nordgren and J.-E. Rubensson, *J. Electron Spectrosc.*, 2013, **188**, 3–9.
- 153 K. Kunnus, I. Josefsson, S. Schreck, W. Quevedo, P. S. Miedema, S. Techert, F. M. F. de Groot, M. Odelius, P. Wernet and A. Föhlisch, *J. Phys. Chem. B*, 2013, **117**, 16512–16521.
- 154 A. Pietzsch, F. Hennies, P. S. Miedema, B. Kennedy, J. Schlappa, T. Schmitt, V. N. Strocov and A. Föhlisch, *Phys. Rev. Lett.*, 2015, **114**, 088302.
- 155 S. Eckert, J. Norell, P. S. Miedema, M. Beye, M. Fondell, W. Quevedo, B. Kennedy, M. Hantschmann, A. Pietzsch, B. E. Van Kuiken, M. Ross, M. P. Minitti, S. P. Moeller, W. F. Schlotter, M. Khalil, M. Odelius and A. Föhlisch, *Angew. Chem., Int. Ed.*, 2017, **56**, 6088–6092.
- 156 A. W. Hahn, B. E. Van Kuiken, V. G. Chilkuri, N. Levin, E. Bill, T. Weyhermüller, A. Nicolaou, J. Miyawaki, Y. Harada and S. DeBeer, *Inorg. Chem.*, 2018, **57**, 9515–9530.
- 157 R. H. Temperton, S. T. Skowron, K. Handrup, A. J. Gibson, A. Nicolaou, N. Jaouen, E. Besley and J. N. O'Shea, *J. Chem. Phys.*, 2019, **151**, 074701.
- 158 A. Fouda, L. C. Seitz, D. Hauschild, M. Blum, W. Yang, C. Heske, L. Weinhardt and N. A. Besley, *J. Phys. Chem. Lett.*, 2020, **11**, 7476–7482.
- 159 E. Biasin, D. R. Nascimento, B. I. Poulter, B. Abraham, K. Kunnus, A. T. Garcia-Esparza, S. H. Nowak, T. Kroll, R. W. Schoenlein and R. Alonso-Mori, *et al.*, *Chem. Sci.*, 2021, **12**, 3713–3725.
- 160 A. Kotani and S. Shin, *Rev. Mod. Phys.*, 2001, **73**, 203–246.
- 161 R. Faber and S. Coriani, *J. Chem. Theory Comput.*, 2019, **15**, 520–528.
- 162 R. Faber and S. Coriani, *Phys. Chem. Chem. Phys.*, 2020, **22**, 2642–2647.
- 163 K. D. Nanda, M. L. Vidal, R. Faber, S. Coriani and A. I. Krylov, *Phys. Chem. Chem. Phys.*, 2020, **22**, 2629–2641.
- 164 K. D. Nanda and A. I. Krylov, *J. Chem. Phys.*, 2020, **152**, 244118.
- 165 D. R. Rehn, A. Dreuw and P. Norman, *J. Chem. Theory Comput.*, 2017, **13**, 5552–5559.
- 166 I. Josefsson, K. Kunnus, S. Schreck, A. Föhlisch, F. de Groot, P. Wernet and M. Odelius, *J. Phys. Chem. Lett.*, 2012, **3**, 3565–3570.
- 167 D. Maganas, S. DeBeer and F. Neese, *Inorg. Chem.*, 2017, **56**, 11819–11836.
- 168 N. Ferré, M. Filatov, M. Huix-Rotllant and C. Adamo, *Density-functional methods for excited states*, Springer, 2016.
- 169 M. W. D. Hanson-Heine, M. W. George and N. A. Besley, *J. Chem. Phys.*, 2017, **146**, 094106.
- 170 A. E. A. Fouda, G. I. Purnell and N. A. Besley, *J. Chem. Theory Comput.*, 2018, **14**, 2586–2595.
- 171 N. A. Besley, *Acc. Chem. Res.*, 2020, **53**, 1306–1315.
- 172 E. Dalgaard, *Phys. Rev. A: At., Mol., Opt. Phys.*, 1982, **26**, 42–52.
- 173 S. M. Parker, S. Roy and F. Furche, *J. Chem. Phys.*, 2016, **145**, 134105.
- 174 S. M. Parker, D. Rappoport and F. Furche, *J. Chem. Theory Comput.*, 2018, **14**, 807–819.
- 175 D. N. Bowman, J. C. Asher, S. A. Fischer, C. J. Cramer and N. Govind, *Phys. Chem. Chem. Phys.*, 2017, **19**, 27452–27462.
- 176 E. C. Alguire, Q. Ou and J. E. Subotnik, *J. Phys. Chem. B*, 2015, **119**, 7140–7149.
- 177 X. Zhang and J. M. Herbert, *J. Chem. Phys.*, 2014, **141**, 064104.
- 178 Q. Ou, G. D. Bellchambers, F. Furche and J. E. Subotnik, *J. Chem. Phys.*, 2015, **142**, 064114.
- 179 Q. Ou, E. C. Alguire and J. E. Subotnik, *J. Phys. Chem. B*, 2015, **119**, 7150–7161.



- 180 X. Zhang and J. M. Herbert, *J. Chem. Phys.*, 2015, **142**, 064109.
- 181 X. Sheng, H. Zhu, K. Yin, J. Chen, J. Wang, C. Wang, J. Shao and F. Chen, *J. Phys. Chem. C*, 2020, **124**, 4693–4700.
- 182 V. V. da Cruz, S. Eckert and A. Föhlisch, *Phys. Chem. Chem. Phys.*, 2021, **23**, 1835–1848, DOI: [10.1039/D0CP04726K](https://doi.org/10.1039/D0CP04726K).
- 183 D. R. Nascimento, E. Biasin, B. I. Poulter, M. Khalil, D. Sokaras and N. Govind, *J. Chem. Theory Comput.*, 2021, **17**, 3031–3038.
- 184 N. T. Maitra, *J. Chem. Phys.*, 2016, **144**, 220901.
- 185 J. M. Herbert, 2022, arXiv preprint arXiv:2204.10135.
- 186 Y. Zhang, W. Hua, K. Bennett and S. Mukamel, *Density-Functional Methods for Excited States*, 2014, pp. 273–345.
- 187 F. Segatta, M. Russo, D. R. Nascimento, D. Presti, F. Rigodanza, A. Nenov, A. Bonvicini, A. Arcioni, S. Mukamel and M. Maiuri, *et al.*, *J. Chem. Theory Comput.*, 2021, **17**, 7134–7145.

